

Article

Study of Landfalling Typhoon Potential Maximum Gale Forecasting in South China

Zhizhong Su ^{1,2}, Lifang Li ^{3,4}, Fumin Ren ^{3,*}, Jing Zhu ^{1,2}, Chunxia Liu ⁴, Qilin Wan ⁴, Qiongbo Sun ¹ and Li Jia ³

¹ Xiamen Key Laboratory of Straits Meteorology, Xiamen Meteorological Bureau, Xiamen 361012, China; shixinqianli@163.com (Z.S.); zhujing_2015@163.com (J.Z.); xmqxsb@163.com (Q.S.)

² Fujian Key Laboratory of Severe Weather, Fujian Meteorological Bureau, Fuzhou 350001, China

³ State Key Laboratory of Severe Weather, Chinese Academy of Meteorological Sciences, Beijing 100081, China; lilifqxx@163.com (L.L.); jl07070522@126.com (L.J.)

⁴ Guangzhou Institute of Tropical and Marine Meteorology, Guangzhou 510080, China

* Correspondence: fmren@163.com; Tel.: +86-1391-032-4105

Abstract: Based on historical tropical cyclone (TC) tracking data and wind data from observation stations, four comparison experiments were designed that considered TC translation speed similarity and five new ensemble schemes in an improved Dynamical-Statistical-Analog Ensemble Forecast (DSAEF) model for Landfalling Typhoon Gale (LTG), which was tested in terms of forecast capability in South China. The results showed that the improved DSAEF_LTG model with the incorporation of TC translation speed and a new ensemble scheme could improve the forecast threat score (TS) and reduce both the false alarm ratio and the missing ratio in comparison with corresponding values attained before the improvement. The TS of the new ensemble scheme model (DLTG_3) was 0.34 at threshold above Beaufort Scale 7, which was 31% better than that of the unimproved model (DLTG_1). At a threshold above Beaufort Scale 10, the TS of DLTG_3 indicated even greater improvement, reaching 0.25, i.e., 127% higher than that of DLTG_1. The results of the experiments illustrated the marked improvement achievable when using the new ensemble scheme. The reasons for the differences in the DSAEF_LTG model forecasts before and after the introduction of TC translation speed and the new ensemble scheme were analyzed for the cases of Typhoon Haima and Typhoon Hato.

Keywords: DSAEF_LTG model; landfalling typhoon gale; parameters improvement; South China



Citation: Su, Z.; Li, L.; Ren, F.; Zhu, J.; Liu, C.; Wan, Q.; Sun, Q.; Jia, L. Study of Landfalling Typhoon Potential Maximum Gale Forecasting in South China. *Atmosphere* **2023**, *14*, 888. <https://doi.org/10.3390/atmos14050888>

Academic Editors: Qinglan Li and Corene Matyas

Received: 13 March 2023

Revised: 14 May 2023

Accepted: 18 May 2023

Published: 19 May 2023



Copyright: © 2023 by the authors. Licensee MDPI, Basel, Switzerland. This article is an open access article distributed under the terms and conditions of the Creative Commons Attribution (CC BY) license (<https://creativecommons.org/licenses/by/4.0/>).

1. Introduction

Tropical cyclones (TCs), which include typhoons, are low-pressure vortices that occur over the surface of a tropical or subtropical ocean and often cause heavy rainfall, strong winds, and storm surges [1]. Annually, approximately 15 TCs affect China, of which approximately seven make direct landfall, making China one of the countries in the world affected most seriously by TC-related disasters [2]. Landfalling TCs accompanied by strong winds, which can trigger storm surges and rainfall that can further aggravate heavy rainfall disasters, represent a disaster-causing factor that cannot be ignored [3]. Super Typhoon Rammasun (2014), which was the strongest typhoon ever recorded to make landfall in China [4,5], had characteristics of multiple landings, rapid intensification, and maintained intensity. The maximum wind speed near the TC center reached 72 m/s when it first made landfall in Wenchang, Hainan Province [6]. Rammasun caused damage to 59 counties and many urban areas with direct economic losses of approximately CNY 26.55 billion. Super Typhoon Meranti (2016) made landfall in Xiamen (Fujian Province) on 15 September 2016. The actual instantaneous wind force measured at the landing site is 63.7 m/s, and the average wind speed in the center reached about 48 m/s. The typhoon caused 650,000 trees in Xiamen to fall down; six 220-V large towers and 45 110-kV substations were destroyed; more than 800 houses collapsed; and 5348 dams were damaged [7]. With the recent rapid economic development, growth in number of buildings, and increase in population density in coastal areas of Southeast China,

the impact of wind damage caused by TCs has become even more serious [8]. Therefore, accurate and timely forecasting of TC-related wind is of considerable regional importance. Additionally, owing to an insufficient understanding of the fine structure of TC gales and an imperfect knowledge of the physical mechanisms of their evolution, TC gale forecasting remains challenging, and its accuracy is inadequate to meet the needs of strategic developments intended to prevent and mitigate TC-related damage [9].

The development of TC gale forecasting technology can be summarized as follows: subjective forecasts, statistical forecasts, numerical forecasts, and the interpretation of numerical forecasts [10]. Subjective forecasts mainly rely on the experience of forecasters and developments in atmospheric sounding technology, as well as the application of satellite cloud maps, radar images, and other information, which have improved the capability of subjective forecasting of TC gales to a considerable extent. Based on historical data, the statistical forecasting approach establishes connections between physical quantities related to TC gales (e.g., wind speed and wind circle radius) and those factors that affect TC gales. Common statistical methods include regression forecasting [11], objective similarity forecasting [12], and climatology and persistence forecasting [13,14]. Numerical model forecasting is an indispensable tool in current TC forecasting operations. Many forecasting agencies have developed numerical forecasting products related to TC gales, and they are gradually developing toward higher resolution and greater refinement [15,16]. The interpretation of numerical forecast products, i.e., the localized and refined interpretation of numerical forecast products to revise errors in numerical forecasts to a certain extent, can be divided into categories of dynamical interpretation [17], statistical interpretation [18], and artificial intelligence interpretation [19] according to the interpretation technique.

Ren et al. [20] have paid attention to the issue of using the combination of dynamical-statistical methods based on similarity forecasts to improve the weather and climate forecasting. They have explored the physical basis of atmospheric similarity problems, starting from the initial values of perfect model, proposing the concept of perfect initial value perturbations, and then proposing the Dynamical–Statistical–Analog Ensemble Forecast (DSAEF) theory. The DSAEF's principle is to use perfect models for forecasting and implement through ensemble forecasting. Li et al. [21] summarized the advantages and shortcomings of the above forecasting methods and showed that the DSAEF theory could provide new ideas for TC gale forecasting by combining the dynamical model and statistical method. Given that the maximum gale during TC affecting land could be used to predict the intensity and extent of TC wind damage [22], Chen et al. [23] initially developed a DSAEF model for a Landfalling Typhoon Gale (LTG) based on the DSAEF theory. To investigate the forecast capability of this model, Li et al. [24] conducted the initial forecast application of the DSAEF_LTG model based on 21 TCs that affected South China. The results showed that the overall forecast performance of the DSAEF_LTG model at thresholds above Beaufort Scale 7 and 10 had advantages over other numerical models (e.g., the CMA, ECMWF, JMA, and NCEP models). However, the DSAEF_LTG model showed a high false alarm ratio (FAR), and for a sideswiping TC with small-scale gales, the DSAEF_LTG model tended to overpredict and failed to achieve satisfactory forecasting results.

The DSAEF_LTG model is in its early stage of development, and there are only three similarity screening factors (i.e., TC track, intensity, and landfall time) considered in the model. The ensemble scheme only has mean and maximum values, and other factors that affect the typhoon potential maximum gale remain to be considered in the DSAEF_LTG model. Jia et al. [25] and Su et al. [26] applied the DSAEF theory to the DSAEF Landfalling Typhoon Precipitation (LTP) model, and their results showed that the incorporation of translation speed similarity and an ensemble forecasting scheme could effectively improve the threat score (TS) of model precipitation forecasts and reduce both the FAR and the missing ratio (MR). Therefore, it is worthwhile investigating whether the abovementioned factors and improvement methods, demonstrated as successful for the DSAEF_LTP model, could also be applicable to the DSAEF_LTG model. To this end, this study conducted an experiment to try to improve the DSAEF_LTG model for South China by introducing the TC

translation speed similarity and ensemble forecast improvements to verify the applicability of the abovementioned improvement methods.

2. Data and Methods

2.1. Data

Historical observed wind speed data were obtained from the National Meteorological Information Center of the China Meteorological Administration (CMA). The data comprised hourly 2-min average wind data at 10-m height from 1980–2018. To ensure data continuity, stations with accumulated missing measurements for more than one year were excluded, and stations at a height above the mean of 894.7 m were excluded to reduce their influence on the TC gale separation results. Finally, data recorded at 140 stations in South China (Guangdong, Guangxi, and Hainan provinces) were retained (Figure 1). It should be noted that the TC potential maximum gale for each station is expressed as the maximum hourly 2-min average wind speed during the period of influence of a single TC.

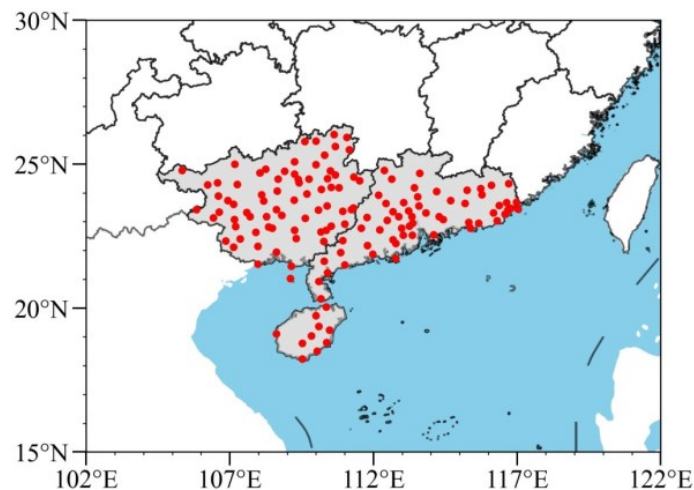


Figure 1. Distribution of the 140 observation stations (red dots) in South China (Guangxi, Guangdong, and Hainan provinces) considered in this study.

Historical TC track information was obtained from the best track dataset of the Shanghai Typhoon Institute of the CMA (<https://tcdata.typhoon.org.cn>) accessed on 1 May 2022, and the data included TC position and intensity at 6-h intervals for the period from 1960–2018. The forecast track and intensity data of the target TCs considered in our experiment were obtained from the expert revised track forecast information based on the numerical forecast model of the CMA.

2.2. Methods

2.2.1. DSAEF_LTG Model

The DSAEF_LTG model adopts the biggest advantage, predicted TC track, of the numerical model as the dynamic part by discriminating the similarity of physical factors affecting LTG and using the gale of the most similar TCs to obtain ensemble LTG forecast of the target TC. It has four main steps: (1) Obtaining the forecast track of the target TC; (2) Establishing the generalized initial values based on the TC track, TC intensity, and other relevant TC characteristics; (3) Using the generalized initial values to determine the similarity between the target TC and historical TCs; and (4) Generating an ensemble prediction of the potential maximum gale of the target TC. A flow chart of the DSAEF_LTG model can be found in Li et al. [24]. Table 1 lists the physical meanings and values of the nine characteristic parameters involved in the above forecasting process. The forecasting procedures and details of the parameters can be summarized as follows. First, the observed track of the target TC before the initial time (P1) and the forecasted track of the target TC

are combined to form the complete track of the target TC. Then, the objective TC track similarity area index (TSAI) is calculated between the target TC and all historical TCs within the established similarity area [27] (P2) and arranged in ascending order. A smaller TSAI value indicates greater similarity between the two types of tracks. In this step, P1–P4 jointly determines the track similarity between the target TC and the historical TC. Based on TC track similarity, historically similar TCs with large differences between the target TC and the historical TC are removed using the conditions from P5–P6 in turn. Finally, the ensemble scheme (P9) is used to assemble the historical TC wind fields corresponding to the selected best similar TCs (the number is determined by P8) to obtain the potential maximum gale forecast results for the target TC. For a single TC, each parameter has multiple values, and different parameters can be combined as a scheme. Therefore, the random combination of parameters can generate 302.4-million forecast schemes under ideal conditions.

Table 1. Parameters of the DSAEF_LTG model.

Parameters	Description	Number of Values
Initial time (P1)	1: 1200 UTC on Day1, 2: 0000 UTC on Day 1, 3: 1200 UTC on Day 2, 4: 0000 UTC on Day 2. (Day 1: the day of TC gale occurring on land; Day 2: the day before Day 1)	$2 \times 2 = 4$
Similarity region (P2)	Parameters of TSAI with rectangular shape. Its southeastern vertex (C) can be the TC position at 00, 12, 24, 36, or 48 h prior to the initial time, and the northwestern vertex (A) can be the TC position at 00, 06, or 12 h prior to the maximum lead time. The 1st–15th values are combinations of C and A. The 16th–20th values are based on the first value, i.e., C represents the TC position at the initial time and A represents the TC position at the maximum lead time. Further details regarding the 16th–20th values can be found in Jia et al. [25]	20
Threshold of the segmentation ratio of a latitude extreme point (P3)	A parameter of the TSAI: 1: 0.1; 2: 0.2; 3: 0.3	3
The overlapping percentage threshold of two TC tracks (P4)	A parameter of the TSAI: 1: 0.9; 2: 0.8; 3: 0.7; 4: 0.6; 5: 0.5; 6: 0.4	6
Seasonal similarity (P5)	A parameter indicating the TC landfall date: 1: entire year; 2: May–November; 3: July–September 4: same landfall month as the target TC 5: within 15 d of the target TC landfall time	5
Intensity similarity (P6)	Four categories 1: average intensity on the first windy day 2: maximum intensity on the first windy day 3: average intensity on all windy days 4: maximum intensity on all windy days	4×5
Translation speed similarity (P7)	Five levels 1: all grades; 2: the target TC intensity is the same grade or above that of the historical TC; 3: the same grade or below; 4: only the same grade 5: the same grade or one grade different Three categories: 1. Average TC translation speed on the first windy day * 2. Minimum average TC translation speed on the first windy day * 3. Average TC translation speed on all windy days * Two Grading criteria: 1. mean *; 2. K-means clustering* Five levels: 1: all grades *; 2: the target TC intensity is the same grade or above that of the historical TC *; 3: the same grade or below *; 4: only the same grade *; 5: the same grade or one grade different *	30

Table 1. *Cont.*

Parameters	Description	Number of Values
Number (N) of analog TCs screened for the ensemble forecast (P8)	1–10 for 1, 2, . . . , 10, respectively	10
Ensemble forecast scheme (P9)	1. mean;	7
	2. maximum;	
	3. 90th percentile *;	
	4. fuse *;	
	5. probability matching mean (PM) *;	
	6. equal difference-weighted mean (ED-WM) *;	
	7. TSAI-weighted mean (TSAI-WM) *.	
Total number of schemes	$4 \times 20 \times 3 \times 6 \times 5 \times 20 \times 30 \times 10 \times 7$	302,400,000

* New methods in this study.

2.2.2. Two Improvements of the DSAEF_LTG Model

Previous studies [28,29] showed that TC translation speed is one of the important factors affecting the maximum gale of a TC. Therefore, it is meaningful to explore the role of TC translation speed similarities for model improvement through experimentation. The steps of adding the TC translation speed similarity factor to the DSAEF_LTG model are as follows. First, the selectable translation speed indicators are determined. Based on 198 translation speed and maximum single-station gale data affecting TCs in South China, the correlation coefficients between six TC translation speed indicators and the maximum single-station process gale of a TC were calculated (Table 2). It can be observed that the correlation coefficients of the first day’s average TC translation speed, the first day’s minimum TC translation speed, and the average TC translation speed are >0.12, and they pass the 0.1 significance level. Consequently, they are identified as the TC translation speed indicators introduced into the model. The second step is to set five levels of relationship in TC translation speed between the target TC and the historical TC (i.e., all levels, same level and above, same level and below, same level only, and maximum difference of one level) to filter similar historical TCs. To ensure that the five TC translation speed level relationships are not duplicated or cover all the level relationships, the three translation speed indicators are divided into seven grades. The third step is to determine the grading criteria of the TC translation speed indicators. Here, average segmentation sorted the TC translation speed first and then divided them into seven continuous intervals with the same sample amount, and the K-means clustering algorithm is used to count the TC translation speed of different levels of the cut-off points. The results are shown in Table 3. Finally, the TC translation speed similarity factor is successfully introduced into the DSAEF_LTG model. Speed similarity can be used in the DSAEF_LTG model by the newly added p7 [30].

Table 2. Correlation coefficients of six TC translation speed indicators with a single-station TC potential maximum gale.

TC Translation Speed Indicator	Single-Station TC Potential Maximum Gale
Average TC translation speed on the first windy day	0.1254 *
Maximum TC translation speed on the first windy day	0.0531
Minimum TC translation speed on the first windy day	0.1809 *
Average TC translation speed on all windy days	0.1201 *
Maximum TC translation speed on all windy days	0.1077
Minimum TC translation speed on all windy days	0.0390

* Significant correlation at the 0.1 level (bilateral).

The ensemble scheme directly affects and determines the forecast results of the DSAEF_LTG model. The mean and maximum ensemble schemes of the original DSAEF_LTG model tend to lead to high FAR and MR scores, indicating the need for new ensemble schemes to be introduced into the model. Referring to the studies of Jia et al. [25] and Ma et al. [31] on the

DSAEF_LTP model, this study introduced five new ensemble schemes into the DSAEF_LTG model: the 90th percentile, Fuse, probability matching mean (PM), equal difference-weighted mean (ED-WM), and TSAI-weighted mean (TSAI-WM) schemes (Table 4).

Table 3. Grading criteria for three types of TC translation speed indicator.

TC Translation Speed Indicator	Method	TC Translation Speed of Cut-Off Points (km/h)						
First day’s average translation speed	Average segmentation	12.79	14.82	17.16	19.63	22.38	26.37	12.79
	K-means clustering	6.83	11.42	15.51	19.39	23.7	28.34	6.83
First day’s minimum translation speed	Average segmentation	8.19	11.38	12.97	15.19	18.02	20.48	8.19
	K-means clustering	1.73	5.82	10.22	15.47	21.63	28.02	1.73
Average translation speed	Average segmentation	12.95	15.22	17.96	20.1	22.7	26.08	12.95
	K-means clustering	11.79	16.18	20.1	23.62	27.61	31.9	11.79

Table 4. New ensemble schemes introduced into the DSAEF_LTG model.

Name	Computational Procedure
90th percentile	For each station, Gale (i), $i = 1, 2, \dots, m$, where m is sorted from minimum to maximum. Gale (r) is the potential maximum gale ranked r. $d = 1 + (m - 1) \times 0.9$ The integer part of d is r and the decimal part is f $Gales = Gale(r) + [Gale(r + 1) - Gale(r)] \times f$
Fuse	Calculation rules of forecast potential maximum gale at each station: If $Max(Gale(i)) \geq 24.5m/s$, Gales = $Max(Gale(i))$; If the 90% percentile values of Gale(i) $\geq 17.2 m/s$, Gales = the 90% percentile value of Gale(i); If the 75% percentile values of Gale(i) $\geq 17.2 m/s$, Gales = the 75% percentile value of Gale(i); If the median value of Gale(i) $\geq 10.8m/s$, Gales = the median value of Gale(i); If none of the above happen, Gales = the 10% percentile value.
Probability matching mean (PM)	All gale data for m members of 140 stations were arranged in ascending order (containing gale data for $140 \times n$ stations). The data were divided into 140 equal parts from $140 \times n$ maximum to minimum, and the median of each part was retained as glm(k), $k = 1, 2, \dots, 140$. Averaging Gale(i) over each station, ranking the average values from largest to smallest, and recording the position of each value in the series. Corresponding to the glm(k) of each station based on the k of each station, and glm(k) is the predicted gale for this station, gale = glm(k).
Equal difference-weighted mean (ED-WM)	The weight of the potential maximum gale for the selected similar TC, the similarity rank I of which is: $W(i) = \frac{(2 \times m - i) \times 2}{(3 \times m - 1) \times m}$ ($i = 1, 2, \dots, m$), $Gales = \sum_{i=1}^m W(i) \times Gale(i)$.
TSAI-weighted mean (TSAI-WM).	$A(i) = \frac{1}{TSAI(i)}$ ($i = 1, 2, \dots, m$), the weight of the potential maximum gale for the selected similar TC whose similarity rank i is: $W(i) = \frac{A(i)}{\sum_{i=1}^m A(i)}$, $Gales = \sum_{i=1}^m W(i) \times Gale(i)$.

2.2.3. Other Methods

(1) TC track similarity area index (TSAI)

The TC TSAI [25] determines the similarity of two TC tracks by calculating the geometric area they enclose. The smaller the TSAI value, the greater the similarity of the tracks.

(2) Evaluation methods

To evaluate the DSAEF_LTG model performance in TC potential maximum gale forecasting, the TS, FAR, and MR are used, which can be calculated as follows:

$$TS = \frac{hits}{hits + misses + false\ alarms} \quad (1)$$

$$FAR = \frac{false\ alarms}{hits + false\ alarms} \quad (2)$$

$$MR = \frac{misses}{hits + misses} \quad (3)$$

where *hits* represents the number of stations with correct forecasts (the number of stations with a gale of a certain level both observed and forecast), *misses* is the number of missed stations (the number of stations with a gale of a certain level observed but not forecast), and *false alarms* is the number of stations with a false forecast (the number of stations with a gale of a certain level forecast but not observed). The values of the above three scores are in the range of 0–1. A TS value closer to 1 indicates a higher hit rate and a better forecasting effect; a FAR score closer to 1 indicates a greater number of false alarms; and an MR score closer to 1 indicates more missed alarms.

3. Experimental Design

3.1. Target TC

The target TCs in this study included training samples and independent samples that were used to perform simulation tests and forecast tests, respectively, and their inclusion criterion was that they must have caused severe gale impact (maximum gale: ≥ 17.2 m/s for at least one station) in South China, i.e., the target TCs included but were not limited to those making landfall in South China. Ultimately, 24 TCs that occurred during 2011–2018 were identified based on the selection criterion, 16 of which from 2011–2015 (Figure 2a) were selected as the training sample, and the remaining eight from 2016–2018 (Figure 2b) were used as the sample for the independent forecast test.

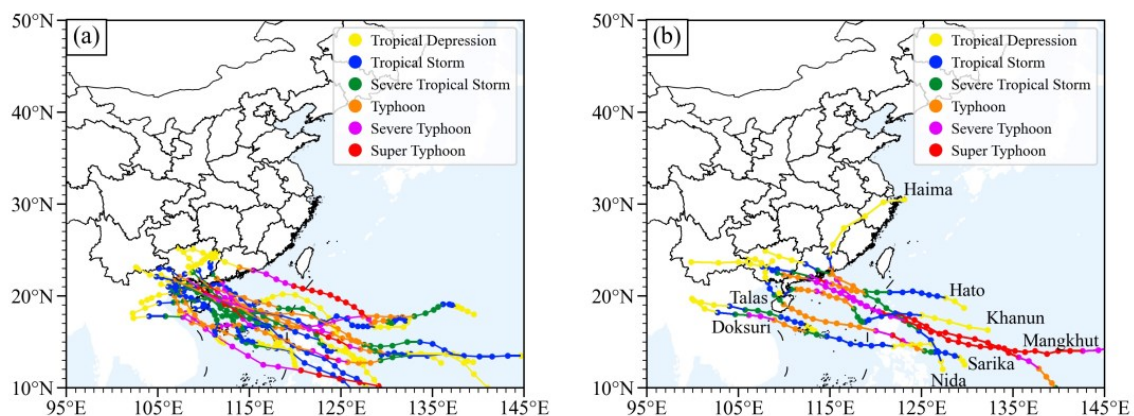


Figure 2. Tracks of (a) the 16 TCs from 2011–2015 selected as the training sample and (b) the eight TCs from 2016–2018 used as the sample for the independent forecast test.

3.2. Improvement Experiments

Four experiments were designed in this study. The first experiment considered the original DSAEF_LTG model without TC translation speed similarity and ensemble scheme improvement (hereafter, DLTG_1). The second experiment involved the model with translation speed similarity only (hereafter, DLTG_2). The third experiment involved the model with the incorporation of an improved ensemble scheme represented by the above five new

ensemble schemes (hereafter, DLTG_3). The fourth experiment involved the model with both translation speed similarity and the five new ensemble schemes (hereafter DLTG_4). The procedure used to determine the best scheme was as follows. First, the best forecast scheme was selected as the optimum one from the training sample when first screening out the forecast schemes common to all 16 TCs, and then selecting the best forecast scheme from the common solution based on certain criteria (e.g., TS maximum). Because the number of similar regions could be limited by the short track of the target TC, or by the number of similar TCs corresponding to the location of the target TC being too small, some TCs could not realize all the forecast schemes. Therefore, the number of common schemes of the 16 training samples was often fewer than the maximum number of schemes possible.

Considering that the TC potential maximum gale of the training samples is concentrated from the Beaufort Scale 6–8 (figure omitted), the TS of the TC potential maximum gale greater than the Beaufort Scale 6 and 8 is denoted as TS6 and TS8, respectively, and the maximum value of their sum (TS6 + TS8; hereafter, TSsum) is used as the selection criterion for the best forecast scheme in their simulation experiment for more effective selection. However, the experiment for independent samples focused on Beaufort Scale 7 and 10 because Beaufort Scale 7 is related to TC scale and Beaufort Scale 10 is a critical reference for TC defense [32]. The meteorological department in China issues early warnings for government guidance and public awareness based on information from observation stations affected by TC gales at thresholds of Beaufort Scale 7 and 10. Additionally, because the forecast performance of the DLTG_1 model (compared with dynamical models such as the CMA, ECMWF, JMA, and NCEP models) has been fully compared and tested by Li et al. [24], and because the independent samples used in this study included two more cases than used in [24], the experiments in this study were conducted to compare the forecast performance of the improved DSAEF_LTG model (i.e., DLTG_2, 3, and 4) with the unimproved model (DLTG_1) for comparative assessment of forecasting capability.

4. Results

The scatter plots presented in Figure 3 show the TSs of the schemes of the four experiments for the 16 training samples. Each black dot in the figure represents a single scheme, and the horizontal and vertical axes correspond to the TS6 and TS8 values, respectively. The red dot represents the maximum value of TS6 + TS8, which is considered the best forecast scheme. DLTG_1 has the fewest schemes, whereas the number of schemes involved in the improved models increase, and DLTG_4 (adding both translation speed similarity and the five new ensemble schemes) has the greatest number of schemes. The maximum value of TSsum for DLTG_2 is 0.8891, which is higher in comparison with that for DLTG_1 (0.8451), while the maximum value of TSsum for both DLTG_3 and DLTG_4 is 0.9284 (TS6 = 0.4134, TS8 = 0.5148), but note that the number of DLTG_4 partial schemes is better than that of DLTG_3 in TS8, i.e., higher than 0.5148. It indicates that compared with the experiment adding only the new ensemble schemes, the experiment that incorporates both translation speed similarity and the new ensemble schemes failed to produce further improvement in the maximum value of TSsum.

Table 5 lists the parameter values of the best scheme in each of the four experiments. As shown by the TC translation speed similarity taken for DLTG_2 and DLTG_4, the level of which in DLTG_2 is set to the same level and below, while in DLTG_4, any TC translation speed indicator is taken and the level is set to all levels; the TC translation speed similarity factor in DLTG_4 cannot filter the historical TCs and thus influence the final best similar TC results. Comparing the ensemble forecast scheme (P9) and the number of best similar TCs in the four experiments, the P9 taken before the ensemble scheme improvement (DLTG_1 and 2) has the maximum values, and that taken after the ensemble scheme improvement (DLTG_3 and DLTG_4) has the probability matching mean (PM); the number of best similar TCs for the latter is increased by one relative to the former. Further comparison between DLTG_3 and DLTG_4 reveals that the parameter values of both are similar, and that there is only a difference in the value of the translation speed similarity: DLTG_3 is without the parameter

of translation speed similarity, and the translation speed similarity parameter in DLTG_4 includes all categories, all grading criteria, and all levels. Thus, the result indicates that the translation speed similarity parameter does not work as in DLTG_2. It can be assumed that the parameters of DLTG_3 and DLTG_4 take the same values, which further explains the existence of the same TSsum maximum for DLTG_3 and DLTG_4.

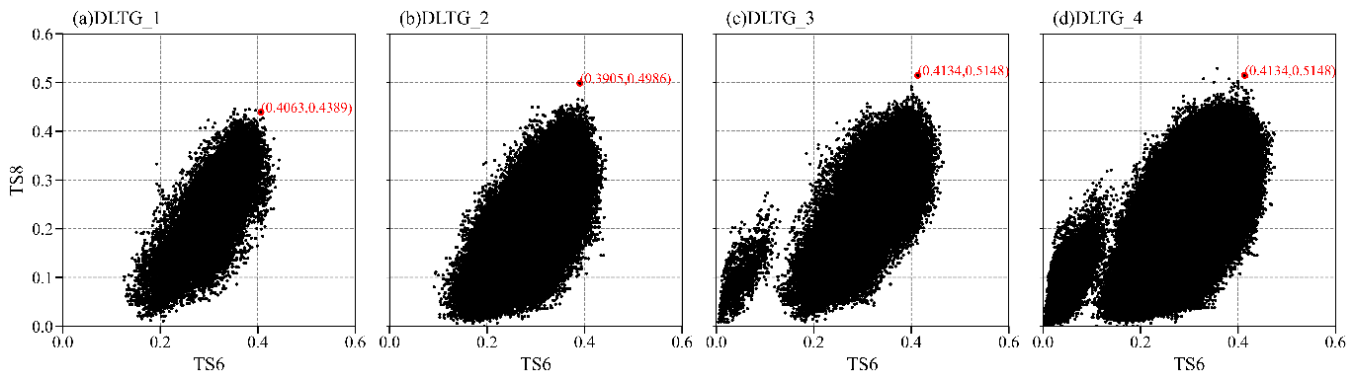


Figure 3. Threat scores of (a) DLTG_1 (unimproved model), (b) DLTG_2 (adding translation speed similarity), (c) DLTG_3 (adding five new ensemble schemes), and (d) DLTG_4 (adding both translation speed similarity and five new ensemble schemes) in the potential maximum gale simulation experiment for 16 training samples. Each black dot represents a single scheme, and the red dot indicates the best scheme with the maximum TSsum (TSsum = TS6 + TS8).

Table 5. Parameter values of the best scheme in the four experiments.

Parameter	DLTG_1	DLTG_2	DLTG_3	DLTG_4
Initial time	3 (1200 UTC on Day 2)	3	3	3
Similarity region	20: shifting A1B1C1D1 (the 16th scheme) to the right by the distance of D1D2 and downward by the distance of B1B2.	16 or 17: (ABCD: the first kind of parameter value of the original similarity region; and A1B1C1D1, a square with side length of 2000 km, is the 16th scheme of the similarity region. The midpoints of B and B1 are taken as B2, and the midpoints of D and D1 are taken as D2, which makes A2B2C2D2 the 17th scheme.	17	17
Threshold of the segmentation ratio of a latitudinal extreme point	2 (0.2)	3 (0.3)	2 (0.2)	2 (0.2)
Overlapping percentage threshold of two TC tracks	5 (0.5)	6 (0.4)	6 (0.4)	6 (0.4)
Seasonal similarity	1 (entire year)	1 or 2 (entire year or May–November)	1 or 2	1 or 2
Intensity similarity	2/5 (maximum intensity on the first windy day/the same grade or one grade different)	1/5 (1: average intensity on the first windy day/the same grade or one grade different)	1/5	1/5
Translation speed similarity	/	2/2/3 (minimum TC translation speed on the first windy day/K-means clustering/the same grade or below)	/	1–3/1–2/1 (all categories /all grading criteria/all levels)
Number (N) of analog TCs screened for the ensemble forecast	2	2	3	3
Ensemble forecast scheme	2 (maximum)	2	7 (probability matching mean (PM))	7

In summary, the results of the training sample simulations show that the TSsum of the best scheme was improved either by adding the translation speed similarity or the new ensemble schemes to the original model alone, or by introducing both improvements. The

TSsum of the best scheme and the parameter values for DLTG_3 and DLTG_4 indicate that the TC translation speed similarity has no effect on the simulation results when the two improvements are introduced simultaneously, i.e., it fails to realize further enhancement of the simulation capability of the model based on the ensemble scheme improvements.

After obtaining the best schemes for the four training experiments, the four schemes were used to forecast eight individual typhoon cases from 2015–2018, and the forecast results were compared. In the process of finding the best scheme for each experiment mentioned above, it was found that the parameters of the best schemes of DLTG_3 and DLTG_4 take similar values, and that the TSsum of the best scheme was the same for both. In the tests with independent samples, DLTG_3 and DLTG_4 demonstrated the same forecast skill, while the results produced by adding the TC translation speed similarity and the new ensemble forecast schemes were the same as those obtained using only the new ensemble forecast schemes without the superimposed improvement effect, which further indicates that the TC translation speed similarity improvement effect cannot be highlighted at this time. For convenient description, the TSs of TC potential maximum gale greater than Beaufort Scale 7 and 10 are denoted TS7 and TS10, respectively. Similarly, the FAR and MR scores of TC potential maximum gale greater than Beaufort Scale 7 and 10 are denoted as FAR7 and FAR10, and as MR7 and MR10, respectively. Above Beaufort Scale 7, the introduction of either the TC translation speed similarity (DLTG_2) or the new ensemble forecast schemes (DLTG_3) can improve the TS of the model (Figure 4), and the improvement of DLTG_3 is greater than that of DLTG_2, i.e., the TS of DLTG_1, DLTG_2, and DLTG_3 is 0.26, 0.3, and 0.34, respectively. This improvement is greater than 31% over the original scheme (DLTG_1). The same comparison results were produced for the case above Beaufort Scale 10. Although the TS decreased in all experiments at Beaufort Scale 10, in comparison with the TS at Beaufort Scale 7, the improvement in the TS for DLTG_3 (0.25) was greater, i.e., an increase of 127% over DLTG_1. This indicates that the DLTG_3 test demonstrated better forecast capability in terms of TC potential maximum gale in more extreme cases. It was also found that the improved model reduced the FAR and MR scores, i.e., the improvement of DLTG_3 (and 4) was greater, where FAR7 and FAR10 were reduced by 0.1214 and 0.2611, respectively, and MR7 was reduced by 0.072. The above analysis indicates that the improved model produces a better forecast and has lower FAR and MR scores as the Beaufort Scale of the TC potential maximum gale increases, reflecting the advantages of the improved model in terms of forecasting TC extreme gales.

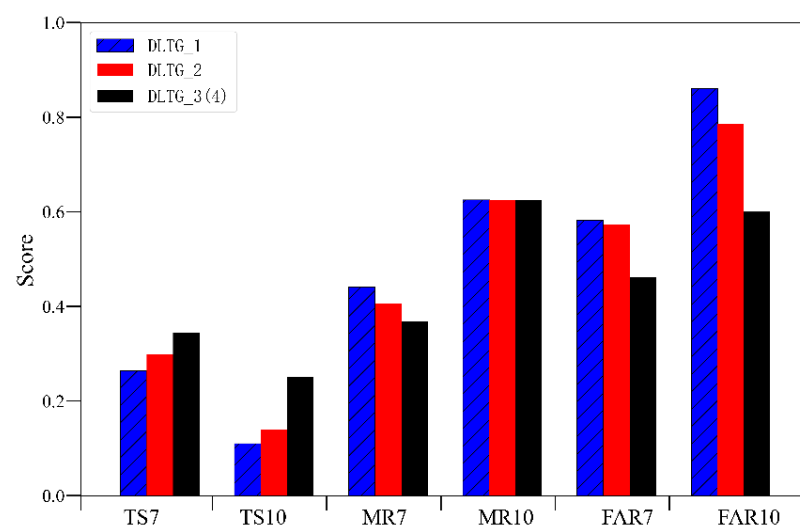


Figure 4. Comparison of the values of the TS, FAR, and MR of the DSAEF_LTG model for the four experiments.

This study also investigated the performance of the four experiments for each TC in the independent forecast sample. At the threshold of Beaufort Scale 7 (Figure 5a), the

improved model increased the TSs for all TCs in comparison with the original model, except for Typhoon Khunan. DLTG_2–4 improved the forecasting capability for sideswiping TCs (e.g., Talas and Doksuri), with the greatest improvement in TS7 for Typhoon Talas (from 0–0.3333). The introduction of the TC translation speed similarity greatly weakened the forecasting capability of the model for Typhoon Sarika and Typhoon Haima, which had a TS7 that decreased by 0.1618 and 0.2069, respectively. The TS7 of most independent samples improved after adding the new ensemble schemes, except that of Typhoon Nida and Typhoon Khanun, for which the TS7 decreased slightly (≤ 0.05). On the comparison between the TC translation speed similarity (DLTG_2) and adding the new ensemble schemes of DLTG_3 (and 4), the TS of DLTG_3 (and 4) lagged behind that of DLTG_2 for three typhoons, and the TS7 of DLTG_3 (and 4) exceeded that of DLTG_2 for the remaining five typhoons. At the threshold of Beaufort Scale 10 (Figure 5b), only Typhoon Hato and Typhoon Mangkhut produced TSs in the four experiments, and it can be seen that the TSs of the improved model were greatly enhanced; specifically, DLTG_3 (and 4) exceeded DLTG_1 and DLTG_2 for both typhoon cases. In summary, the results demonstrate that the ensemble scheme improvement has a greater impact on model performance.

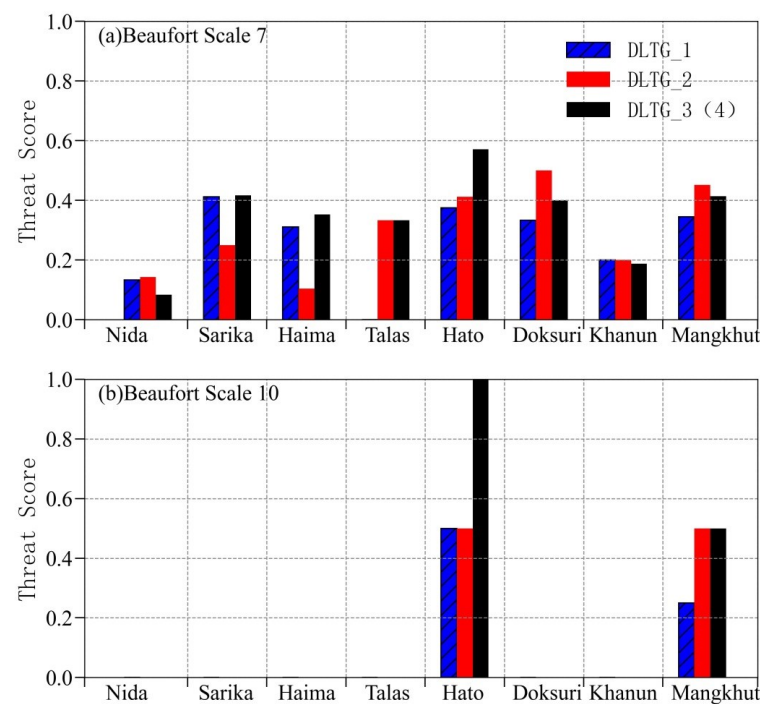


Figure 5. Comparison of the TS in the four DSAEF_LTG model experiments for each TC in the independent forecast experiments: (a) Beaufort Scale 7 and (b) Beaufort Scale 10.

To analyze the reasons for the large differences in forecast capability after the introduction of the TC translation speed similarity factor and the new ensemble schemes, the cases of Typhoon Haima and Typhoon Hato with the largest TS differences between DLTG_3 (and 4) and DLTG_2 at Beaufort Scale 7 and Beaufort Scale 10, respectively, were examined. Typhoon Haima had the largest TS increase in the DLTG_3 (and 4) test in comparison with the DLTG_2 test at Beaufort Scale 7. Figure 6 shows that the observations of maximum gale during Typhoon Haima (Figure 6a) were mainly distributed in eastern Guangdong Province, and that the extreme center was located off the coast of Chaoshan. None of the experiments forecasted a gale greater than Beaufort Scale 10 at Chaoshan. However, for other levels of gale, the potential maximum gale of DLTG_1 (Figure 6b) produced more stations with a gale between Beaufort Scale 7 and Beaufort Scale 10 in the central coastal area of Guangdong Province, and the FAR of the gale extreme center was high. For DLTG_2 (Figure 6c), a similar TC (8926) made landfall in the south of Hainan Island, for which use of the ensemble forecast scheme resulted in a gale in a region that

deviated severely from the observations. The overall forecast had severe FAR and MR scores. It can be seen from Figure 6d that this TC was also one of the most similar TCs in DLTG_3 (and 4), but it did not cause the gale in Hainan Province, and the MR score of the wind field was also improved in comparison with that of DLTG_1. Moreover, the distribution of the gale between Beaufort Scale 7 and Beaufort Scale 10 fitted more closely to the observations in eastern coastal areas of Guangdong province, mainly because the probability matching mean (PM) ensemble method was used to adjust and redistribute the gale field of the three similar TCs, thereby making it more reasonable.

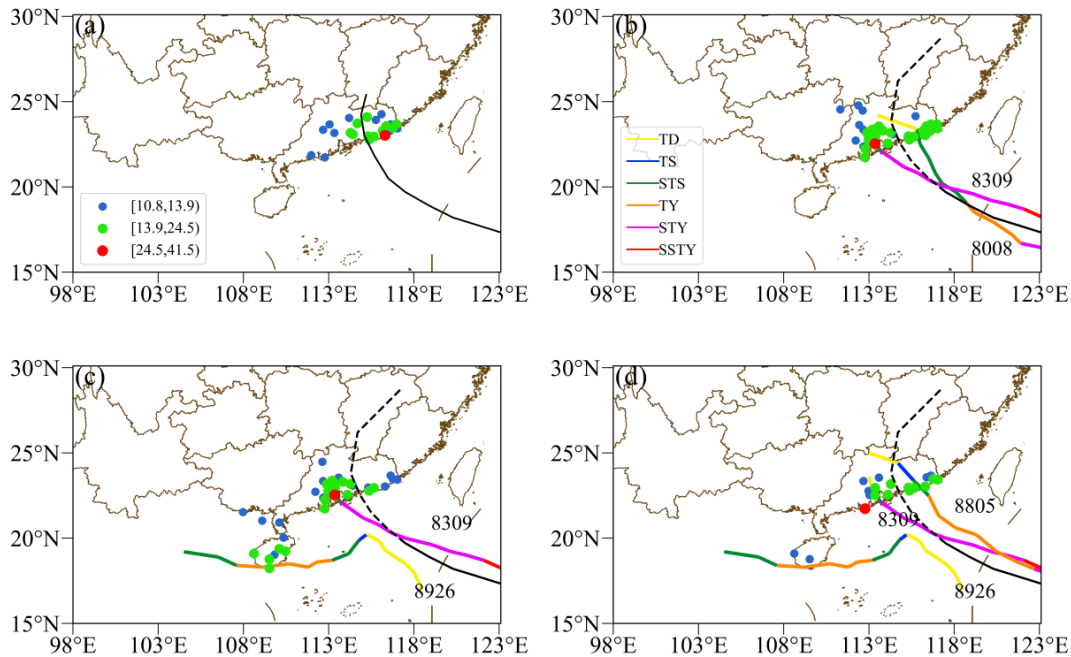


Figure 6. Distribution of potential maximum gale (m/s) during Typhoon Haima according to (a) observations; (b) DLTG_1; (c) DLTG_2; and (d) DLTG_3 (and 4). Black solid line is the observed track, black dashed line is the forecasted track, and colored solid line is the best similar TC track. (The first two digits of in the figure stand for the last two numbers of the year, and the last two digits stand for the number of the typhoon in that year. For example, “8926” stands for typhoon No. 26 in 1986).

Typhoon Hato was the strongest TC to make landfall in Guangdong Province in 2017, and it caused exceptional gale damage to the western coast region of the Pearl River Estuary, with wind speeds of up to Beaufort Scale 15 recorded in the city of Macau [33]. The gale observations of Typhoon Hato (Figure 7a) were mainly distributed along the western coast of the Pearl River Estuary, with the extreme center located off the coast of Macau, similar to the forecast gale of DLTG_1 near the time of landfall (Figure 7b). The morphology is close to the observations, but there is a false alarm station at Beaufort Scale 10 on the left side of the typhoon track. In DLTG_2 (Figure 7c), the false alarm station at Beaufort Scale 10 remains on the left side of the typhoon track, but the distribution of stations at Beaufort Scale 7 on the right side of the track is closer to the track, which is more consistent with the observations. For DLTG_3 (and 4) (Figure 7d), the forecast of a gale greater than Beaufort Scale 10 near the time of landfall on the left side of the typhoon track is the same as the observations, and the FAR7 is improved substantially. It can be seen that the DLTG_2 test that adopted the ensemble scheme of the maximum method inevitably led to the false potential maximum gale greater than Beaufort Scale 10; the DLTG_3 (and 4) test identified one more similar typhoon case (8903) in comparison with DLTG_2, and after adopting the probability matched average ensemble method, the forecast magnitude of the gale at some stations was reduced, which made the adjusted gale field distribution more reasonable and improved the TS at the threshold of Beaufort Scale 10.

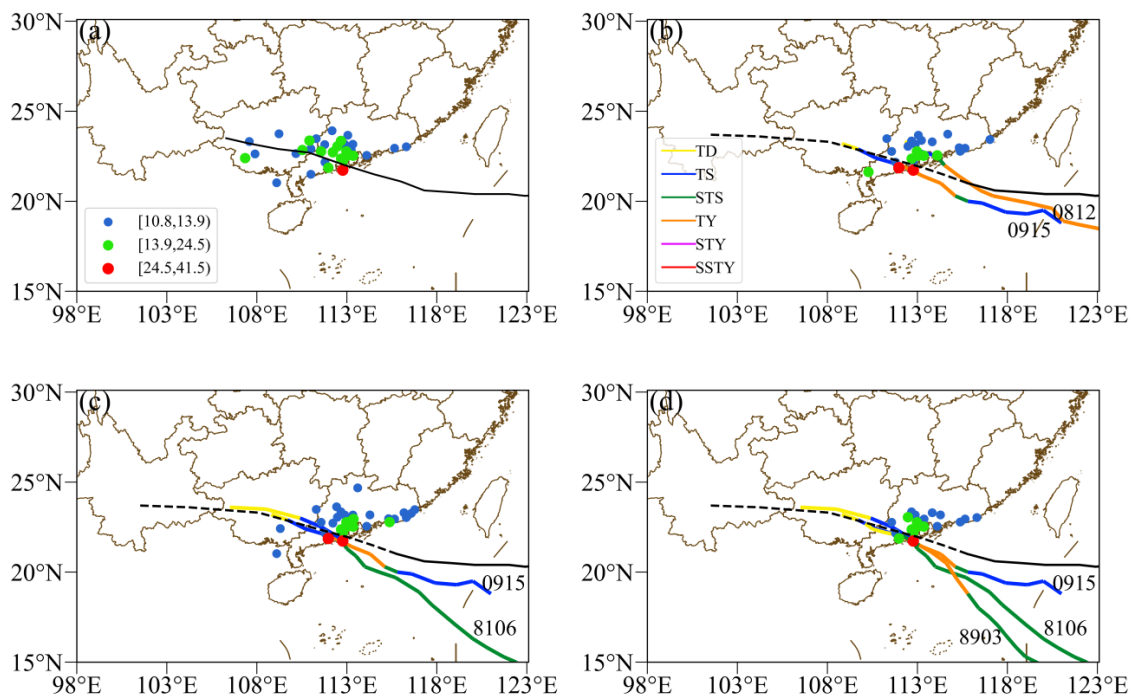


Figure 7. Distribution of potential maximum gale (m/s) during Typhoon Hato according to (a) observations; (b) DLTG_1; (c) DLTG_2; and (d) DLTG_3 (and 4). Black solid line is the observed track, black dashed line is the forecasted track, and colored solid line is the best similar TC track.

5. Conclusions

In this study, four experiments were designed by adding TC translation speed similarity and five new ensemble methods to the DSAEF_LTG model. The best forecast scheme in these experiments was determined by selecting 16 TCs that affected South China during 2011–2015 as training samples and conducting independent sample forecast tests for eight TCs that affected China during 2016–2018, to test the forecast effects of the best scheme for each experiment. The derived conclusions are as follows.

- (1) The training sample experiments showed that the introduction of TC translation speed similarity or improvement of the ensemble scheme separately showed marked improvement effects, and that the TSsum reached 0.8891 and 0.9284, respectively, which exceeded that of the unimproved model (0.8451). However, when the two improvements were introduced simultaneously, the introduction of the TC translation speed similarity did not produce an improvement effect. Further analysis of the model parameter values revealed that introduction of TC translation speed similarity has no impact on the results when simultaneously adding a new ensemble scheme in the DSAEF_LTG model.
- (2) The results of the independent sample forecasting experiments showed that the DSAEF_LTG model can be improved by adding TC translation speed similarity or by adding new ensemble schemes; the TS was 0.26 for a gale greater than Beaufort Scale 7, and the TS was 0.34 when adding a new ensemble scheme, i.e., 31% higher than that of the original ensemble scheme. Moreover, the FAR and MR scores also decreased in comparison with those realized before the model improvement. The improved TS of the ensemble scheme reached 0.25, i.e., 127% higher than the TS of the original scheme, reflecting the advantage of the model for extreme typhoon gales greater than Beaufort Scale 10.
- (3) The results of the independent sample forecasting experiments also showed that when TC translation speed similarity and new ensemble schemes are introduced simultaneously, the forecasting effect is the same as that when the TC translation speed similarity is introduced alone, with a TS of 0.35 (0.25) for a gale at the threshold of

Beaufort Scale 7 (Beaufort Scale 10). The ensemble scheme improvement can adjust the gale fields of multiple similar TCs, which makes the forecast results more reasonable. This potentially explains why the model performs better after the ensemble scheme improvement than after the introduction of TC translation speed similarity.

This study considered South China as the target research area, which is a region affected frequently by TCs. Based on the DSAEF_LTG model improvement test, it can be seen that adopting a reasonable ensemble scheme and increasing the generalized initial similarity factor simulation is an important approach for improving the model simulation capability. The effects of different model improvement methods on the results were shown to vary, and when multiple improvement methods were introduced simultaneously, some methods had limited improvement effect and did not demonstrate the effect of superimposed improvement, which should be investigated further in the future. Furthermore, the current physical similarity factors considered in the DSAEF_LTG model still lack inherent TC features, such as a TC scale. Therefore, future research will continue to improve the model to enhance the forecasting capability of the DSAEF_LTG model in terms of the potential maximum gale.

Author Contributions: Conceptualization, Z.S., F.R. and C.L.; Data curation, J.Z. and Q.S.; Formal analysis, Z.S. and Q.W.; Methodology, L.L., F.R. and L.J.; Software, L.J.; Supervision, F.R. and C.L.; Visualization, Q.S. and L.J.; Writing—original draft, Z.S. and L.L.; Writing—review & editing, Z.S., L.L., J.Z. and Q.W. All authors have read and agreed to the published version of the manuscript.

Funding: This research was funded by Guangdong Province Key Research and Development Project (No. 2019B111101002), Shenzhen Science and Technology Q11 Project (No. KCXFZ2020122173610028), Xiamen Science and Technology Program (No. 3502Z20206078), the Natural Science Foundation of Fujian Province, China (No. 2022J01445, 2021J01464 and 2021J01458), and the Major Science and Technology Projects of Fujian Key Laboratory of Severe Weather (No. 2022TF02).

Institutional Review Board Statement: Not applicable.

Informed Consent Statement: Not applicable.

Data Availability Statement: The datasets generated during and/or analyzed during the current study are available from the corresponding author upon reasonable request.

Acknowledgments: The authors thank the Key Innovation Team of Marine Meteorological Disaster Mechanisms and Forecasting Technology of Fujian Meteorological Bureau for technical support and financial support. The authors thank the National Meteorological Information Center of CMA and STI of CMA for making the wind observation data and TC tracks data available. The authors also thank the anonymous reviewers, whose comments help to improve the quality of this manuscript.

Conflicts of Interest: The authors declare no conflict of interest.

References

1. Peduzzi, P.; Chatenoux, B.; Dao, H.; Bono, A.D. Global trends in tropical cyclone risk. *Nat. Clim. Change* **2012**, *2*, 289–294. [[CrossRef](#)]
2. Chen, L.S.; Duan, Y.H.; Song, Y.L.; Xu, Y.L. *Typhoon Forecast and Its Disasters*; Meteorological Press: Beijing, China, 2012; pp. 2–3.
3. Powell, M.D.; Reinhold, T.A. Predicting Tropical Cyclone Destructive Potential by Integrated Kinetic Energy According to the Powell/Reinhold Scale. U.S. Patent US7970543 B2, 28 June 2011.
4. Zhou, Y.; Ni, Z.; Vetter, P.A.; Xu, H.; Hong, B.; Wang, H.; Li, W.; Liu, S. Model Simulation of StormSurge in the Northwestern South China Sea Under the Impact of Sea Level Rise: A Case Study of Super Typhoon Rammasun (2014). *Front. Mar. Sci.* **2022**, *9*, 878301. [[CrossRef](#)]
5. Wang, Q.; Xu, Y.; Wei, N.; Wang, S.; Hu, H. Forecast and service performance on rapidly intensification process of Typhoons Rammasun (2014) and Hato (2017). *Trop. Cyclone Res. Rev.* **2019**, *8*, 18–26. [[CrossRef](#)]
6. Zhang, X.; Wei, N.; Wang, Q. Influence of radiation diurnal variation on the rapid intensification process of super Typhoon Rammasun (1409) in the South China Sea. *Front. Earth Sci.* **2022**, *10*, 940418. [[CrossRef](#)]
7. Zhang, L.J.; Li, L.S. People-oriented emergency response mechanism—An example of the emergency work when typhoon Meranti stroked Xiamen. *Int. J. Disaster Risk Reduct.* **2019**, *38*, 101185. [[CrossRef](#)]
8. Yu, J.H.; Xue, H.X.; Song, J. Tropical cyclone potential hazard in Southeast China and its linkage with the East Asian westerly jet. *Asia-Pac. J. Atmos. Sci.* **2017**, *53*, 295–304. [[CrossRef](#)]

9. Qian, C.H.; Duan, Y.H.; Ma, S.H. The current status and future development of China operational typhoon forecasting and its key technologies. *Adv. Meteorol. Sci. Technol.* **2012**, *2*, 36–43.
10. Dong, Y. *Distribution Characteristics and Forecast of Tropical Cyclone Gales in Guangxi*; Guangxi Normal University: Guangxi, China, 2014.
11. Messner, J.W.; Mayr, G.J. Probabilistic Forecasts Using Analogs in the Idealized Lorenz96 Setting. *Mon. Weather Rev.* **2011**, *139*, 1960–1971. [[CrossRef](#)]
12. Wilson, K.A.; Gallo, B.T.; Skinner, P.; Clark, A.; Heinselman, P.; Choate, J.J. Analysis of End User Access of Warn-on-Forecast Guidance Products during an Experimental Forecasting Task. *Weather Clim. Soc.* **2021**, *13*, 859–874. [[CrossRef](#)]
13. Knaff, J.A.; Sampson, C.R.; Demaria, M. Statistical Tropical Cyclone Wind Radii Prediction Using Climatology and Persistence. *Weather Forecast.* **2007**, *22*, 781–791. [[CrossRef](#)]
14. Knaff, J.A.; Sampson, C.R.; Musgrave, D. Statistical tropical cyclone wind radii prediction using climatology and persistence: Updates for the western north Pacific. *Weather Forecast.* **2018**, *33*, 1093–1098. [[CrossRef](#)]
15. Demaria, M.; Knaff, J.A.; Knabb, R. A new method for estimating tropical cyclone wind speed probabilities. *Weather Forecast.* **2009**, *24*, 1573–1591. [[CrossRef](#)]
16. DeMaria, M.; Knaff, J.; Brennan, M.J.; Brown, D.P.; Knabb, R.D.; DeMaria, R.T.; Schumacher, A.B.; Lauer, C.A.; Roberts, D.P.; Sampson, C.R.; et al. Improvements to the operational tropical cyclone wind speed probability model. *Weather Forecast.* **2013**, *28*, 586–602. [[CrossRef](#)]
17. Hoover, B.T.; Morgan, M.C. Validation of a Tropical Cyclone Steering Response Function with a Barotropic Adjoint Model. *J. Atmos. Sci.* **2010**, *67*, 1806–1816. [[CrossRef](#)]
18. Maini, P.; Kumar, A.; Rathore, L.S.; Singh, S.V. Forecasting Maximum and Minimum Temperatures by Statistical Interpretation of Numerical Weather Prediction Model Output. *Weather Forecast.* **2003**, *18*, 938–952. [[CrossRef](#)]
19. Sun, J.B.; Qian, Y.Z.; Chen, P.Y.; Zheng, Z.; Le, Y.L. The Artificial Neural Network Method on the Station Wind in Landfall Typhoon. *Meteorol. Mon.* **2010**, *36*, 81–86.
20. Ren, F.; Ding, C.; Zhang, D.-L.; Chen, D.; Ren, H.-L.; Qiu, W. A Dynamical-Statistical-Analog Ensemble Forecast Model: Theory and An Application to Heavy Rainfall Forecasts of Landfalling Tropical Cyclones. *Mon. Weather Rev.* **2020**, *148*, 1503–1517. [[CrossRef](#)]
21. Li, L.F.; Ren, F.M.; Liu, C.X.; Wan, Q.L. Overview of research advances in forecasting of typhoon gale. *J. Mar. Meteorol.* **2022**, *42*, 50. [[CrossRef](#)]
22. Titley, H.A.; Cloke, H.L.; Harrigan, S.; Pappenberger, F.; Prudhomme, C.; Robbins, J.C.; Stephens, E.M.; Zsoter, E. Key Factors Influencing the Severity of Fluvial Flood Hazard from Tropical Cyclones. *J. Hydrometeor.* **2021**, *22*, 1801–1817. [[CrossRef](#)]
23. Chen, Y.X. *DSAEF_LTG Model Study of Dynamic-Statistical Similar Ensemble Prediction of Landfall Tropical Cyclone Gales*; Chengdu University of Information Technology: Chengdu, China, 2020.
24. Li, L.; Chen, Y.; Ren, F.; Liu, C.; Ma, Y.; Wan, Q. Experiment with the dynamical–statistical–analog ensemble forecast model for landfalling typhoon gale over South China. *Front. Earth Sci.* **2022**, *10*, 987001. [[CrossRef](#)]
25. Jia, L.; Ren, F.; Ding, C.; Jia, Z.; Wang, M.; Chen, Y.; Feng, T. Improvement of the ensemble methods in the dynamical–statistical–analog ensemble forecast model for landfalling typhoon precipitation. *J. Meteorol. Soc. Jpn.* **2022**, *100*, 575–592. [[CrossRef](#)]
26. Su, Z.; Ma, Y.; Jia, L.; Ren, F.; Ding, C. Application of the improved dynamical–Statistical–Analog ensemble forecast model for landfalling typhoon precipitation in Fujian province. *Front. Earth Sci.* **2023**, *10*, 1018851. [[CrossRef](#)]
27. Ren, F.; Qiu, W.; Ding, C.; Jiang, X.; Wu, L.; Xu, Y.; Duan, Y. An objective track similarity index and its preliminary application to predicting precipitation of landfalling tropical cyclones. *Weather Forecast.* **2018**, *33*, 1725–1742. [[CrossRef](#)]
28. Rupp, J.A.; Lander, M.A. A Technique for Estimating Recurrence Intervals of Tropical Cyclone-Related High Winds in the Tropics: Results for Guam. *J. Appl. Meteor. Climatol.* **1996**, *35*, 627–637. [[CrossRef](#)]
29. Cao, C.; Wang, Z.D.; Zheng, F. Causal Analysis of Strong Wind Weather in Zhejiang Induced by Typhoon Morakot. *Meteorol. Sci. Technol.* **2013**, *41*, 1109–1115. [[CrossRef](#)]
30. Jia, L.; Ren, F.; Ding, C.; Wang, M. Improving the Forecast Performance of the DSAEF_LTP Model by Incorporating TC Translation Speed Similarity. *Weather Forecast.* **2022**, *37*, 1855–1865. [[CrossRef](#)]
31. Ma, Y.Q.; Ren, F.M.; Jia, L.; Ding, C.C. Experiments with the improved dynamical–statistical–analog ensemble forecast model for landfalling typhoon precipitation over South China. *J. Trop. Meteorol.* **2022**, *28*, 139–153. [[CrossRef](#)]
32. Sampson, C.R.; Knaff, J.A. A consensus forecast for tropical cyclone gale wind radii. *Weather Forecast.* **2015**, *30*, 1397–1403. [[CrossRef](#)]
33. Zhao, Y.J.; Li, J.N.; Dong, X.H.; Feng, Y. The impact of resolution on the simulation results of typhoon hatu (2017). *J. Trop. Meteorol.* **2019**, *35*, 629–643. [[CrossRef](#)]

Disclaimer/Publisher’s Note: The statements, opinions and data contained in all publications are solely those of the individual author(s) and contributor(s) and not of MDPI and/or the editor(s). MDPI and/or the editor(s) disclaim responsibility for any injury to people or property resulting from any ideas, methods, instructions or products referred to in the content.